Telescopic Time-Scale Bridging for Modeling Dispersion in Rapidly Oscillating Flows

Ram K. Balachandran
Dept. of Mechanical Engineering, University of Minnesota, Minneapolis, MN 55455

Jaijeet Roychowdhury
Dept. of Electrical Engineering and Computer Sciences, University of California, Berkeley, CA 94720

Kevin D. Dorfman
Dept. of Chemical Engineering and Materials Science, University of Minnesota, Minneapolis, MN 55455

Victor H. Barocas
Dept. of Biomedical Engineering, University of Minnesota, Minneapolis, MN 55455

Analytical solution of dispersion in rapidly oscillating flows becomes infeasible in complex geometries. Simulation over long durations can be prohibitively expensive when there is a wide separation between the oscillation and dispersion time scales. Here, we present a methodology based on an implicit envelope-tracking scheme coupled with telescopic projections. A test problem, with a known analytical solution, was simulated, and the effect of Péclet number on the dispersivities was investigated. The solution was unaffected by the time steps for telescopic projections while increasing Péclet numbers introduced errors. The error was found to decrease with mesh refinement, but a small inherent error was observed. The method was also applied to a practical problem of interest to us: drug dispersion due to sloshing in the vitreous humor of the eye. Relative to single-scale solution, the method, when applied to the vitreous sloshing problem, produced speedup values of up to 100. © 2011 American Institute of Chemical Engineers AIChE J, 58: 1987–1997, 2012
Keywords: saccadic motion, envelope tracking, vitreous liquefaction

Introduction

Alteration of molecular transport in the presence of fluid flow has been studied for decades. The effect of convection on diffusional transport of molecules was famously studied by Taylor,[1] who showed that mass transport is enhanced in the presence of a steady Poiseuille flow in a pipe. Since then, numerous studies[2–7] have been performed on the topic of enhanced diffusion/dispersion induced by variety of flows on different geometries. Analytical solutions for many simple geometries are available in literature. Aris[8] considered the effect of pulsations in the flow and evaluated the effective dispersion coefficient in pulsatile flow through a circular tube. Dispersion was due to a periodic velocity field induced by pulsating pressure gradients. The work by Aris laid the foundation for subsequent work by Horn,[9] who evaluated the effective dispersion coefficient for a solute diffusing between two parallel plates, infinite in extent, with fluid between them. The lower plate was held fixed and the upper plate was oscillated sinusoidally. A detailed explanation of the relevance of Horn's results for our work is given in the article.

The theory of enhanced dispersion in an oscillating velocity field has been used to study, among other topics, transport of gases in bronchial airways[10,11] and methods for separation of gases.[12] High-frequency ventilation, commonly used during acute respiratory failure to ensure continuous O_2 to CO_2 exchange in the lungs, is an important example. Slutsky et al.[13] showed that due to augmented diffusion in the central airways, significant gas transport can be achieved during high-frequency ventilation even with a very small tidal volume. Since then, numerous studies, both experimental and theoretical, have been conducted to evaluate the effective dispersivity for gas transport in bronchial airways during mechanical ventilation. Some studies[14–16] then used the experimentally measured dispersion to create a computational model for gas transport during high-frequency ventilation.

Augmented diffusion in oscillatory flow has also been used to separate molecules and isotopes on a large scale. Dispersion has shown to increase mass transfer by up to six orders of magnitude in the case of liquids and four to five orders for gases.[12] Jaeger et al.[17] have combined the effects of increased mass transfer in oscillatory flow with countercurrent flow to improve separation greatly.

Despite the aforementioned successes, there remain significant challenges. In particular, complex geometries can render analytical solution impossible, and numerical methods

must be used. As will be described in the subsequent paragraphs, a number of impediments to direct numerical simulation exist, but certain advances now enable practical computational simulation of complex dispersion problems.

Convection–diffusion problems become numerically challenging when convection dominates diffusion to the point that the spatial discretization is unable to resolve the mass transport boundary layer. The upwind scheme, one of the numerous remedies available to tackle the problem, was developed by Christie et al.[18] for one-dimensional (1-D) problems and later generalized to the two-dimensional case by Heinrich et al.[19] The method was extended by Brooks et al.,[20] who eliminated the crosswind diffusion introduced by the upwind scheme and modified the method so that the upwind effect acts along the streamlines. The work was one of the seminal articles published, and we refer the readers to a more recent review by the same author for further information.[21] The method amounts to adding an artificial diffusion coefficient along the streamlines to balance out the strength of convection. For 1-D problem, the optimal amount of artificial diffusion balances the numerical inhibition of diffusion inherent in central difference schemes, or the Galerkin finite element method (GFEM) with piecewise linear basis functions, resulting in exact nodal solutions.

Simulation of dispersion in rapidly oscillating flows over long durations, using conventional methods, becomes computationally infeasible when the time scales involved are widely separated. As the frequency of oscillation is often high for such flows, and diffusion is generally slow, the time scale for diffusion can be very large compared to the time period of oscillation. It is not conceptually difficult to simulate long durations with very small time steps, but it would require a prohibitive amount of time even with the use of advanced hardware. Hence, a strategy that makes use of the information provided by both time scales but is not computationally demanding is needed. There is considerable literature available, in domains ranging from circuit simulation to molecular dynamics, on numerical techniques for speeding up oscillatory problems with widely separated time scales. Without providing any detailed review, we refer the interested reader to the following selected works which are directly relevant to the technique we use here.[22–24] The basic idea is to extrapolate slow trends (the "envelope"), obtained via detailed local simulation of a few fast cycles of oscillation, and skip over many fast cycles of oscillation. Finding the next point of the envelope, while skipping cycles of the fast oscillations on which it rides, can be achieved using explicit or implicit numerical methods. A key insight enabling this work, borrowed from the circuit simulation domain,[25] is that implicit schemes for envelope following can provide robustness and efficiency when solving the oscillatory fluid flow problem—even though they require Jacobian information and nonlinear solution at each envelope step and hence are more complicated to implement than explicit schemes. The major objectives of this work were therefore as follows:

• To develop an implicit envelope-tracking methodology to deal with multiscale transport problems in the time domain.

• To compare the numerical solution to the analytical solution for a model problem that involves the essential phenomena of interest, but exists in a simpler geometry, and

• To apply the method to a demonstrative problem involving a complex geometry. Owing to our interest in ophthal-

mic drug delivery,[26,27] we choose the problem of drug dispersion in the vitreous humor (henceforth "vitreous") of the eye. Saccadic (left-right, as in reading) motion of the eye causes sloshing of the vitreous[28–30] which may affect biodistribution of injected or implanted drugs. The presence of the lens introduces geometric complexity, and the time-scale difference between saccades ($\sim$ms) and dispersion ($\sim$h) is significant.

Methods

Solution to the flow problem

We consider a system in which a rapidly oscillating flow of velocity v occurs in an arbitrary geometry, and a species of interest is dispersed within the domain by a combination of convection and diffusion. The first step is to solve the flow problem, given by the incompressible Navier–Stokes equations,

$$\rho \left(\frac{\partial v}{\partial t} + v \cdot \nabla v \right) = \nabla \left(-p\mathbf{I} + \mu \left(\nabla v + (\nabla v)^T \right) \right) \quad (1)$$

$$\nabla \cdot v = 0 \quad (2)$$

and the appropriate boundary conditions (the effect of gravity is absorbed into the pressure term). Many methods, based on the finite element method, exist to solve the flow problem,[31,32] each with various advantages and disadvantages, but our preference is the standard GFEM, which is well-suited to complex geometries and highly successful for low-to-moderate Reynolds numbers. To account for the LBB condition, quadratic and linear interpolation functions were used for the velocity and pressure approximation respectively.[33] For time integration, we use implicit Euler and solve the linearized forms of Eqs. 1 and 2 simultaneously via Multifrontal Massively Parallel Solver (MUMPS).[34]

Solution of the species transport problem

Species transport was modeled using the convection–diffusion equation:

$$\frac{\partial c}{\partial t} + v \cdot \nabla C - D\nabla^2 C = 0, \quad (3)$$

where c represents concentration, D is the diffusion coefficient, and v is the velocity of oscillating flow calculated from Eqs. 1 and 2.

A multimodule C code, based on the GFEM, was developed to solve the fluid-flow problem for velocity and pressure and solve the mass transport problem for concentration. The same geometry and mesh were used for both problems. The periodic motion velocities were calculated beforehand and were used as inputs for the transport problem. Hence, there exists only a one-way coupling between the momentum and species balance equations. Implicit Euler was used for time integration, and MUMPS was used to solve the resulting linear algebraic equations.

The Péclet numbers ($P\acute{e}$; defined as the ratio of convective to diffusive time scales) of interest to us (drug transport in the vitreous) are of the order of 10^6. At such high Péclet numbers, the Galerkin finite element scheme becomes highly unstable, and spurious oscillations in time and space cloud the actual solution unless a highly refined mesh is used.[20] For the method to be stable on its own, there must be a balance between convection and diffusion at the length scale of

an element (i.e., the mesh Péclet number should be order 1). Such refinement would be prohibitive for Péclet numbers as large as ours. To overcome this problem, we used the streamline upwinding method discussed by Brooks et al.[20] The method amounts to adding a balancing/artificial diffusivity to the natural diffusivity, along the streamlines to counterbalance convection, and thereby provide stability.

The optimum amount of artificial diffusion, which results in the exact solution for a 1-D problem solved using the central difference scheme, was calculated by Hughes et al.[35] to be

$$D_{\mathrm{bal}} = \frac{vh}{2}\beta, \tag{4}$$

where β is given by

$$\beta = \coth(\alpha) - 1/\alpha. \tag{5}$$

α in Eq. 5 is given by

$$\alpha = vh/2D. \tag{6}$$

D_{bal} is the balancing diffusivity, v is the velocity, h is the length of the 1-D element, and α is the mesh Péclet number in the above equations. It should be noted that the above calculations for the balancing diffusivity would also hold good for a 1-D Galerkin finite element discretization using piecewise linear basis functions as such a discretization scheme would result in the same set of equations as the central difference scheme.[20] Our problem of interest was three-dimensional in nature and used Galerkin discretization. Hence, we set the net diffusivity (true plus balancing) for our problem to be

$$\boldsymbol{D} = D\mathbf{I} + D_{\mathrm{bal}}\frac{\boldsymbol{v} \otimes \boldsymbol{v}}{|\boldsymbol{v}|^2}, \tag{7}$$

where $\otimes$ denotes dyadic product, and $\boldsymbol{D}$ is the net diffusivity tensor. D_{bal} is given by the following expression:

$$D_{\mathrm{bal}} = \frac{\beta_\xi v_\xi h_\xi + \beta_\eta v_\eta h_\eta + \beta_\zeta v_\zeta h_\zeta}{2} \tag{8}$$

where β_ξ, β_η, and β_ζ are given by

$$\beta_\xi = \coth(\alpha_\xi) - 1/\alpha_\xi, \quad \beta_\eta = \coth(\alpha_\eta) - 1/\alpha_\eta,$$
$$\text{and} \quad \beta_\zeta = \coth(\alpha_\zeta) - 1/\alpha_\zeta. \tag{9}$$

α_ξ, α_η, and α_ζ in Eq. 9 are given by

$$\alpha_\xi = v_\xi h_\xi/2D, \quad \alpha_\eta = v_\eta h_\eta/2D \quad \text{and} \quad \alpha_\zeta = v_\zeta h_\zeta/2D. \tag{10}$$

The quantities h_ξ, h_η, and h_ζ are the dimensions of the element in the three isoparametric directions. Similarly, v_ξ, v_η, and v_ζ and α_ξ, α_η, and α_ζ are the components of the velocity and the mesh Péclet number in the three isoparametric directions. The balancing diffusivity was calculated at the integration points (Gauss points) for each element based on the velocity at the integration point and the element dimensions according to Eqs. 8–10. To assess the error introduced by the artificial diffusivity for a multidimensional discretization with piecewise quadratic basis functions, we simulated the problem discussed by Horn[9] and compared the numerical solution to the analytical solution. A detailed discussion of the test problem is provided toward the end of the section.

The treatment described in the above paragraph was not implemented for the fluid flow problem. The Reynolds number (Re; defined as the ratio of the diffusive to convective time scale for momentum transport) for the flow problem in the vitreous was around 600. At the length scale of a finite element, Re was small enough to allow use of the standard Galerkin method. The Reynolds number stated above was calculated based on a vitreous viscosity of 0.001 Pa·s (viscosity of water). For the simulations of interest, the viscosity of vitreous was varied up to three orders of magnitude higher than that of water and hence the associated Reynolds numbers were small enough that standard Galerkin was sufficient.

Telescopic implicit envelope-tracking scheme

The telescopic implicit envelope-tracking scheme was used to tackle the multiscale nature of the species transport problem. The convective time scale and the time period of oscillation were much smaller than the diffusive time scale. The time period for the rapid oscillations (T) was typically 0.25 s for our problem of interest. The diffusion time scale (τ_d) is given by

$$\tau_\mathrm{d} = \frac{L^2}{D}, \tag{11}$$

where L is the diffusion length scale. For transport of a small molecule in vitreous humor ($L \sim 0.85$ cm; $D \sim 6 \times 10^{-6}$ cm^2 s^{-1}), τ_d is on the order of 30 h. Also, for our problem of interest the convective time scale (τ_c) given by L/v, is of the order of 0.2 s. Conventional time integration schemes would necessitate using time steps on the order of T or τ_c, for which simulating long periods of drug dispersion would be impractical. Hence, there is a need to use effectively the information provided by all the time scales, and at the same time speed up the simulation process.

The concentration, solved from Eq. 3, is expected to oscillate in time as the velocity is periodic in time. As the oscillation is expected to be fast compared to the underlying slow diffusive process, the envelope of these oscillations will be a slowly varying function of time.[22] Hence, the natural strategy would be to track the envelope of the oscillations rather than the fine details of the solution. The envelope for our problem was the path traced by points at the start and end of each period of oscillation. Petzold[22] suggested a method whereby the knowledge of the solution over a few periods is used to estimate the solution at a time point many periods away. The method is illustrated in Figure 1. The solution procedure involves

1. Solving Eq. 3 for $c(t)$ over K periods ($K = 3$ or 4) using the fast time-scale information.

2. Based on the information available over the first K periods, projecting $c(t)$—forward to a point P, M periods away ($M \gg K$).

3. Using the value at P as the initial condition, solving Eq. 3 again over K periods, and repeating steps 2 and 3 to simulate over long durations.

The procedure allowed simulation of transport for up to $M + K$ periods by solving the finite element method (FEM) problem over K periods giving a speedup of $1 + (M/K)$. The extent of M, however, is limited by stability.[36] A fully implicit envelope-tracking method to project to point P (step 2) stabilizes the code better and extends the upper bound of M.
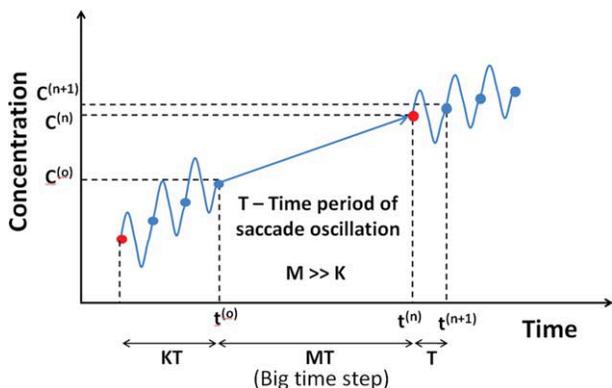
Figure 1. Schematic of the multiscale method proposed by Petzold[22] to bridge the time scales.

[Color figure can be viewed in the online issue, which is available at wileyonlinelibrary.com.]

A fully implicit envelope tracking scheme was used to implement step 2. The scheme was previously applied to oscillators in circuits by Mei et al.[25] The goal of the implicit envelope-tracking scheme was to evaluate the concentration $c^{(n)}$ at the time step n using known information, i.e., $c^{(0)}$ and the concentration at the previous time steps. The slope of the envelope at time step n was used to approximate the slope of the projection step at $c^{(0)}$ as follows:

$$\frac{c^{(n)} - c^{(0)}}{MT} = \frac{c^{(n+1)} - c^{(n)}}{T}. \qquad (12)$$

As $c^{(n+1)}$ can be evaluated by solving Eq. 3 over one period with $c^{(n)}$ as the initial condition we can write

$$c^{(n+1)} = f(c^{(n)}, t^{(n)}). \qquad (13)$$

As the original PDE, Eq. 3, is linear in c, f is a linear function. The initial guess for $c^{(n)}$ was obtained by using an explicit projection, i.e., the slope of the envelope at $c^{(0)}$ was used to approximate the slope of the projection step at $c^{(0)}$ to obtain $c^{(n)}$. Eq. 12 can be rewritten as:

$$R = Ac^{(n)} - c^{(0)} = 0, \qquad (14)$$

where

$$A = (M+1)I - M\frac{\partial c^{(n+1)}}{\partial c^{(n)}}. \qquad (15)$$

Equation 14 was then solved for $c^{(n)}$. I in the above equations is the identity matrix and R is the residual.

If m time steps are used to evaluate $c^{(n+1)}$ from Eq. 3 (see Figure 2), with $c^{(n)}$ as the initial condition, then constructing A would involve m inverse operations and $2m - 1$ matrix–matrix products (details in the Appendix). As the matrices are large, constructing A would be a computationally arduous task, slowing down the projection step and eliminating the speedup possibly obtained from the multiscale strategy. To overcome this problem, we adopted a matrix-free method, taking advantage of the fact that when iterative methods are used to solve the set of linear equations, they require only a matrix–vector product and not the matrix itself. As the matrix A in our problem is a Jacobian, the matrix–vector product can be approximated by

$$Av = \left[\frac{\partial R}{\partial c}\Big|_{c^{(n)}}\right] v = \frac{R(c^{(n)} + \varepsilon v) - R(c^{(n)})}{\varepsilon}, \qquad (16)$$

where ε is a small number. Thus the product is evaluated by evaluating the residual, resulting in a substantial reduction in memory required and more importantly computation time. The generalized minimal residual method (GMRES) with reverse communication, developed by Saad et al.,[37] was used for the linear solve. As f represents change over one period, $\partial c^{(n+1)}/\partial c^{(n)}$ is close to the identity, making the spectral radius of A small. Thus, GMRES converges without preconditioning—a feature that is attractive from a computational, as well as ease-of-implementation, perspective.

To achieve better speedups without compromising on stability, implicit envelope-tracking was combined with telescopic projective methods to push forward in time. Telescopic methods were developed by Gear et al.[38] for stiff differential equations with gaps in their eigenvalue spectrum. Figure 3 illustrates a three-layered projection method that was used in our simulations. As explained in the previous paragraphs, the first (bottom) layer involves solving for the fast time scale solution over K periods and then projecting the solution forward in time over M periods. The procedure is repeated n times and the n solution values (indicated using red dots in Figure 3) calculated are used to take a bigger projection step at the second level. The third level of projections can be calculated in a similar manner. The strategy ensures higher speedup and better stability. The stability of the multilevel telescopic projective method has been shown to be better than single-level projection methods.[39] The procedure results in a maximum speedup of

$$\text{Speedup} = \left(1 + \frac{M}{K}\right)\left(1 + \frac{M}{n}\right)\left(1 + \frac{M}{n}\right), \qquad (17)$$

where n is the number of solution values used for projection from the previous level (Figure 3).

Although the telescopic implicit envelope-tracking scheme provides better stability and speedup, there still exists an upper bound on the value of M. At each level different M values were used to maximize the advantage of the technique without compromising on stability. For simulating drug transport in the vitreous the highest value used for M was 20 (at the third level) and the lowest was 1 (at the first
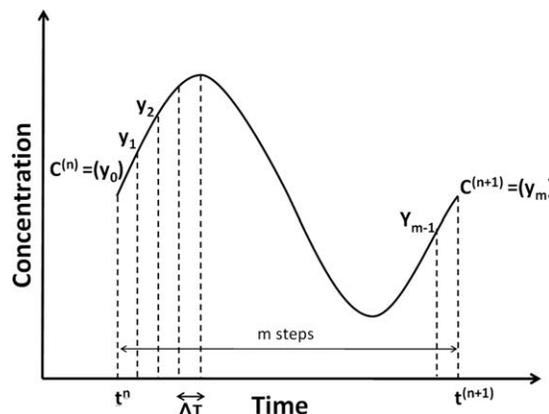

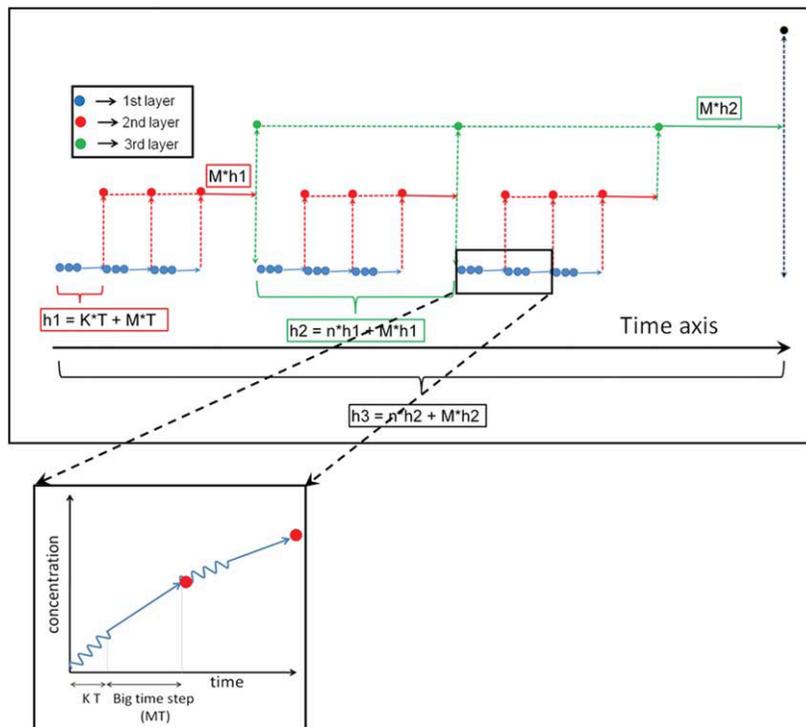**Figure 2. Schematic of the fully implicit envelope-tracking scheme.**

Figure 3. Illustration explaining the telescopic projection technique that was developed by Gear et al.[36]

[Color figure can be viewed in the online issue, which is available at wileyonlinelibrary.com.]

level). Generally, lower values were used initially as steep changes in concentration were observed. Typical K values used in our simulations were 3 and 4, and n was set equal to K.

Test Problem

A test problem with a known analytical solution was solved to assess the error introduced by the telescopic implicit envelope-tracking and the artificial diffusion. Horn's work on mass transport under oscillatory flow conditions[9] provides an ideal test case. The system consists of fluid contained between two infinite, parallel plates separated by a distance H (Figure 4). A Cartesian coordinate system is fixed on the lower plate, with the x direction pointing in the direction of flow and the y direction pointing between the two plates. The upper plate was oscillated with a velocity $V_0 \sin(2\pi\omega t)$, where V_0 is the characteristic value of the speed and ω is the frequency of oscillation. At low Reynolds number, the velocity profile can be assumed to be linear, and hence $\boldsymbol{U} = U\boldsymbol{e_x}$, with the magnitude of flow being

$$U = V_0 \sin(2\pi\omega t)\left(\frac{y}{H}\right). \tag{18}$$

The spread of a tracer, introduced over a small interval of x over the entire y–z-plane at $t = 0$, can be described by a dispersion coefficient (D^*). Horn determined D^* to be

$$\frac{D^*}{D} = 1 + f(\lambda)Pe^2. \tag{19}$$

where

$$f(\lambda) = \frac{\lambda(\cos\ \lambda + \cosh\ \lambda) - (\sin\ \lambda + \sinh\ \lambda)}{8\lambda^5(\cos\ \lambda + \cosh\ \lambda)}, \tag{20}$$

$$\lambda \equiv H\sqrt{\frac{\pi\omega}{D}}, \tag{21}$$

and D is the diffusivity of the tracer in the fluid. The Péclet number for transport (Pe) is defined as

$$Pe \equiv \frac{V_0 H}{D}. \tag{22}$$

The initial spread of the tracer was assumed to be a Gaussian of the form

$$c_0 = \frac{M_0}{2\sqrt{\pi D t_0}} e^{-\left(\frac{x^2}{4Dt_0}\right)}, \tag{23}$$

where c_0 is the initial concentration at $t = 0$, M_0 is the total amount of tracer in the volume initially, and t_0 is a constant. The spread of the tracer as a function of time can be expressed as
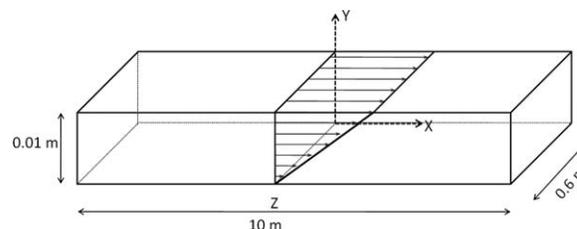

Figure 4. Schematic of the geometry used to model mass transport under oscillatory flow conditions solved by Horn.[9]
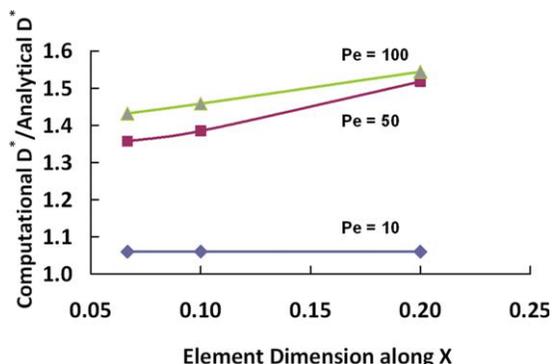
Figure 5. Plot of the effect of mesh refinement on the computed dispersion coefficient for Péclet numbers of 10, 50, and 100 for the test problem.

[Color figure can be viewed in the online issue, which is available at wileyonlinelibrary.com.]

$$\bar{c} = \frac{M_0}{2\sqrt{\pi D^*(t + t_0)}} e^{-\frac{x^2}{4D^*(t+t_0)}}, \qquad (24)$$

where $\bar{c}$ represents the concentration averaged over $0 \le y \le H$ at the start of each time period. The fluxes on all the boundaries were assumed to be zero. The dimensions of the domain were such that the assumptions were deemed acceptable. This was ensured by choosing simulation times that was long compared to diffusion in the y direction but short compared to diffusion in the x-direction.

The test problem was solved over a $10 \times 0.01 \times 0.6$ m³ ($H = 0.01$ m) box (Figure 4) with $D = 1 \times 10^{-7}$ m² s^{-1}, and $\omega = 2 \times 10^{-3}$ s^{-1} and hence, $\lambda = 2.5$. Velocity was adjusted based on the Péclet number. The telescopic implicit envelope-tracking method, described in the previous section, was used to simulate the transport of a tracer, and the computationally evaluated dispersion coefficient was compared with the analytical value for varying test cases to validate the method. The dispersion coefficient was evaluated based on Eqs. 25 and 26. The first (x_0) and second moments (σ^2) of the spread of the tracer, with respect to time were evaluated, and the dispersion coefficient was set to be half the slope of the second moment as follows:

$$D^* = \frac{1}{2}\frac{d(\sigma^2)}{dt}, \qquad (25)$$

where

$$\sigma^2 = \frac{\int c(x - x_0)^2 dx}{\int c\, dx}. \qquad (26)$$

x_0, which was also the mean of the distribution was calculated to be approximately zero.

Drug dispersion in the vitreous humor

A brief discussion of the drug dispersion problem in the vitreous is presented here. The practical problem has been dealt with in greater detail in Ref. 40. The vitreous undergoes progressive liquefaction with age and hence sloshes readily during saccadic motion of the eye.[28] The solution methodology involves solving for the sloshing velocity due to saccadic eye movements and using the velocities to solve the drug transport problem. The fluid flow problem and the species transport problem were solved separately (as in the test problem) with the telescopic implicit envelope-tracking scheme applied only to the species transport problem. The vitreous in its native state is a viscoelastic material,[41] but liquid vitreous loses its elastic properties and hence was assumed to be a purely viscous Newtonian fluid. The viscosity values were varied to simulate various physiological vitreous states. Equations 1 and 2 were modified because the problem was solved in a frame of reference rotating along with the eye. The momentum balance equation was modified by adding additional terms to account for the oscillation of the computational domain with respect to a stationary frame of reference. The modified equation is as follows:

$$\rho\left(\frac{\partial v}{\partial t} + (v \cdot \nabla)v + \Omega \times (\Omega \times r) + 2\Omega \times r + \alpha \times \mathbf{r}\right)$$
$$= \nabla\left(-p\mathbf{I} + \mu(\nabla v + (\nabla v)^T)\right). \qquad (27)$$

In our model, small-amplitude saccades were assumed to cause negligible drug dispersion when compared to the large-amplitude saccades and were neglected. Sloshing caused by continuous saccades of 40° amplitude (modeled using sinusoids) was simulated. Saccade parameters such as amplitude, duration, and peak angular velocity were determined using empirical relationships developed by Becker.[42] The velocities converged to the periodic solution within 4 periods. Drug distribution in the vitreous was modeled using the species balance equation (Eq. 3). The flux of the drug into and out of the vitreous through the retina and the hyaloid (see Figure 7) was calculated based on previously estimated transport properties of the posterior tissues[27] and used as the boundary condition for the model. The details of the calculation involved in the boundary conditions are presented in Ref. 40.

The three-dimensional model, developed based on the geometry of the human eye, was divided into 12,285 hexahedral 27-noded elements with a total of 104,725 nodes. Triquadratic basis functions were used for velocity and concentration, and trilinear basis functions were used for the pressure. To demonstrate the utility of the numerical scheme,
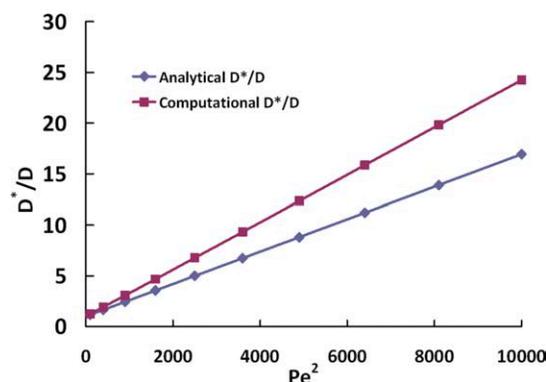

Figure 6. Plot showing the effect of Péclet number (Pe) on the computationally and analytically evaluated dispersion coefficient for the test problem.

[Color figure can be viewed in the online issue, which is available at wileyonlinelibrary.com.]
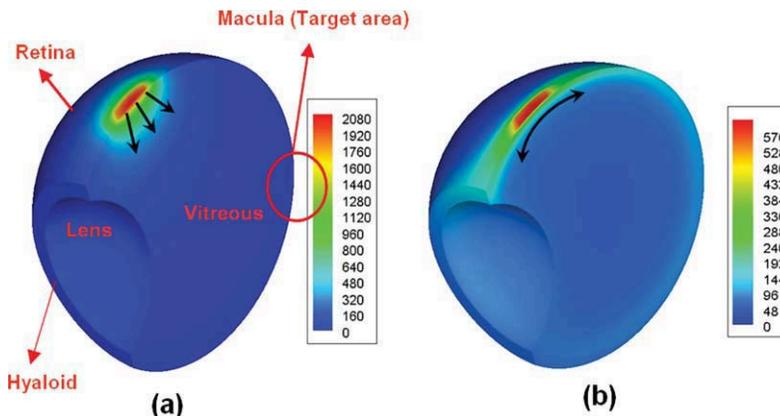
Figure 7. Concentration profile for (a) static and (b) sloshing vitreous after transscleral drug administration.

The figure also highlights the key clearance routes namely, hyaloid and retina and the direction of drug transport for the two cases. [Color figure can be viewed in the online issue, which is available at wileyonlinelibrary.com.]

discussed earlier, for complex geometries, we compare simulation results for drug dispersion in static vs. sloshing vitreous.

Results

Evaluation of the test problem

To assess the performance of the numerical scheme, the dispersion coefficient was evaluated for the test problem, and was compared with the analytical value obtained from Eq. 19. The accuracy of the telescoping time stepping scheme was assessed by varying the values of M at each telescopic layer. As noted before, three layers of projections were used and at each layer the projection step is represented as an integral multiple of the time period of oscillation. For the sake of brevity, we represent the schemes as m_1-m_2-m_3, where

$$m_1 = \frac{MT}{T}, \quad m_2 = \frac{Mh_1}{T}, \quad m_3 = \frac{Mh_2}{T}, \quad (28)$$

and h_1, and h_2 are as illustrated in Figure 3.

Schemes 1-2-2, 1-4-16, and 3-12-60 were used to perform the calculations; very little change in the dispersion coefficient was observed for the three cases when $Pé$ values of 10, 50, and 100 were used. The variation in the dispersion coefficients were less than 0.028% of each other. The simulations were performed on a mesh with 10,000 elements (element dimension along X = 0.10). The result shows that changing the projection steps does not affect the solution adversely. The speedup for the test problem for the 3-12-60 case is 5.56. It should be noted that as the goal was only to assess the scheme for the test problem, the speedups were much lower than those obtained for the vitreous sloshing problem ($\sim$100).

The effect of incorporating an artificial diffusion coefficient on the solution was tested by refining the mesh and comparing the computational D^* to the analytical D^* for varying Péclet numbers. Flow velocities and hence the artificial diffusivity for the test problem were along the X direction (Figure 4). Mesh refinement was done along X and number of elements along Y and Z directions was kept the same. Figures 5 and 6 show the variations. The numerical scheme was always observed to overpredict the dispersivity when compared to the analytical solution, and the error was observed to decrease with mesh refinement especially for high $Pé$. The mesh Péclet

number decreases with mesh refinement, and hence the amount of artificial diffusivity added to balance convective effects is also reduced, reducing the dispersivity. However, at $Pé = 10$, mesh refinement was not observed to reduce the error of about 5% between computational and analytical D^* any further, thereby indicating an inherent error in the numerical scheme. Some possible reasons for the error are given in the discussion section of the article.

Drug dispersion in the vitreous

The model was used to simulate drug delivery to the posterior eye from a constant concentration surface (transscleral) source and from a point (intravitreal) source in the vitreous. The results from the simulations have been discussed in detail elsewhere.[40] Vitreous viscosity was varied from 0.01 to 1.0 Pa s for the simulations. Here, we only present simulation results for a vitreous viscosity of 1.0 Pa s to highlight the practical importance of the results, while the other cases are only discussed briefly. The results for the sloshing vitreous were compared with those for a static vitreous for both types of sources. It should be noted that the static vitreous case is the limiting case when the vitreous viscosity is infinity. Figures 7a, b show the concentration plots for the two cases for a transscleral source. As the species balance
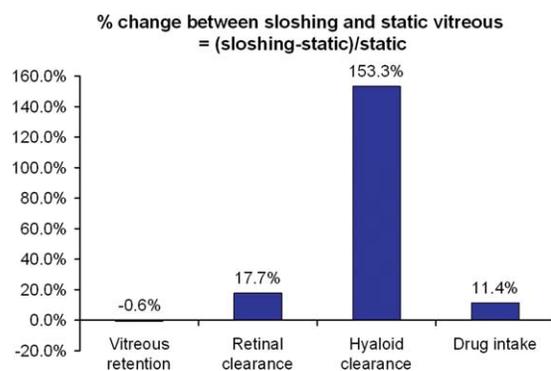

Figure 8. Plot showing the relative differences in drug clearance, retention, and intake for the static and sloshing vitreous after transscleral administration.

[Color figure can be viewed in the online issue, which is available at wileyonlinelibrary.com.]
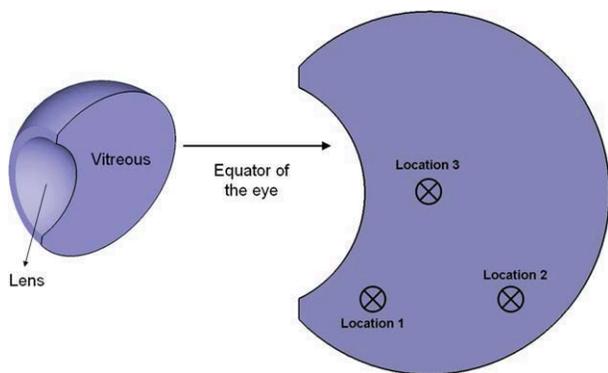
Figure 9. Schematic showing the location of the intravitreal point sources in the equator of the eye.

[Color figure can be viewed in the online issue, which is available at wileyonlinelibrary.com.]

equations were linear equations in concentration (c), arbitrary transscleral source strength of 1×10^{-4} was picked for the simulations. Hence, the plots in Figure 7 are for comparative purposes only. With a constant concentration transscleral source, simulations were run until steady state was reached ($\sim$48 h). Peak vitreous concentration, which was observed directly under the drug source, was higher for the static case when compared to the sloshing case. Also, steep concentration gradients were observed for the static case resulting in lower drug intake for the static case compared to the sloshing case (Figure 8). This also suggests that there is increased mixing of the drug in the sloshing vitreous, as the fluid flow washes away any drug accumulation under the source, resulting in more uniform spreading of drug in the vitreous. The extent of mixing significantly impacted the time scale for transport for sloshing cases where vitreous viscosities were two orders of magnitude lower than that considered here. The time to reach 95% of the steady state value was lower by a factor of 1.5 for the case when the vitreous viscosity was 0.01 Pa s. Increased mixing for the sloshing case resulted in easier access to the clearance routes through the retina and hyaloid. At the hyaloid, the increase in clearance is significantly high due to the flow mixing pattern and the proximity of the drug source to the hyaloid. The flow under the drug source results in spreading of the drug in the tangential direction along the wall as opposed to radial transport for the static vitreous (Figure 7). This effect coupled with the proximity of the drug source to the hyaloid results in high concentrations at the hyaloid, resulting in increased clearance. The increased clearance through the hyaloid and retina outweighed the increase in drug intake, resulting in lower concentrations in the sloshing vitreous. More importantly, the concentration at the macula, which is critical for treating age-related macular degeneration, was observed to be up to nine times higher (not shown in the figures).

The time of retention for the drug delivered through an intravitreal injection (simulated using a Gaussian point source) was also evaluated. Simulations were run for $\sim$13 h, by which time the vitreous levels were almost zero. Three source locations were considered, all on the equator of the globe (Figure 9) to take advantage of symmetry. Figure 10 shows the half-life of the drug source at each location for the static and sloshing vitreous. Retinal clearance accounted for 95% of all drug eliminated from the eye and hence had

the biggest impact on the residual vitreous concentrations. Retinal clearance was high for all the sloshing cases resulting in lower vitreous concentrations when compared to the static case. Sloshing did not have a significant impact on half-life for injections placed closer to the retina as mixing did not result in a significant difference in retinal clearance. For a centrally placed injection, however, mixing due to sloshing resulted in the half-life of drug decreasing by 14%. The effect of sloshing was higher for some of the lower viscosity cases (0.01 Pa s and 0.1 Pa s) that were simulated. For the lower viscosities half-life was found to be independent of location and was $\sim$42% lower than that for the static vitreous for locations 1 and 2, and 63% lower for location 3.

Discussion

Dispersion in rapidly oscillating flows is frequently encountered in a variety of engineering applications. The problem is difficult to handle when complex geometries prohibit the use of analytical techniques and when widely separated time scales present challenges for numerical solvers. The methodology discussed in this article was designed to address such problems.

The numerical scheme was assessed using a test problem with a known analytical solution, and the results were compared for varying Péclet numbers, element size, and time steps for telescopic projections. The time steps used for telescopic projections were observed to have no effect on the evaluated dispersion coefficients. This suggests that the accuracy of the multiscale strategy is not limited by the extent of the time steps and hence, long time simulations are possible at relatively low computational cost. Although not limited by accuracy concerns, the extent of the time steps could be limited by stability. For example, the speedup during the initial part of the simulation of drug dispersion in the vitreous was limited due to steep change in concentration with respect to time. However, once the initial transients stabilized speedups up to 100 were achieved. This was not a concern in the test problem, because of its simplicity. Hence, care should be taken when using large time steps for complex problems, particularly those in which steep changes in concentration can be expected.

The numerical scheme predicts a higher dispersivity for the test problem when compared to the analytically
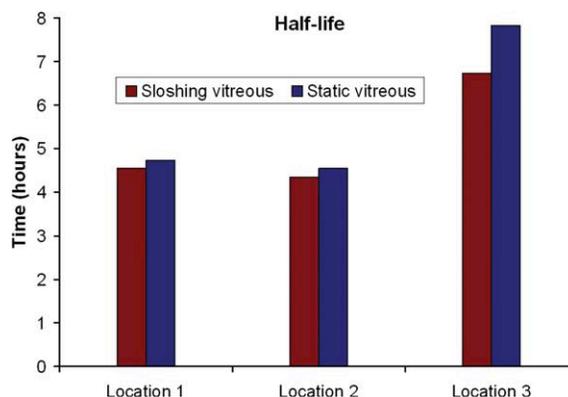

Figure 10. Comparison of half-life values for the static and sloshing vitreous for drug injections at three different locations in the vitreous.

[Color figure can be viewed in the online issue, which is available at wileyonlinelibrary.com.]

evaluated dispersion coefficient as shown in Figures 5 and 6. The method was observed to match the analytical solution within 10% at $P\acute{e} = 10$ and within 40% at $P\acute{e} = 100$. Some of the potential causes for the error are discussed below. Mesh refinement was found to decrease the error but further refinement beyond an element dimension of 0.067 was not attempted. The decrease in error with element size could be partly attributed to the artificial diffusivity. Mesh refinement reduces the mesh Péclet number and hence reduces the amount of artificial diffusivity required to balance the effect of convection. For low Péclet numbers, however, the reduction in error with the size of the element is insignificant, suggesting the presence of an inherent disagreement between the numerical scheme and the analytical solution. The inherent error, observed to be in the 5–10% range, could be due to multiple sources. One possible source of error is the finite size of the computational domain, in contrast to the infinite domain for the analytical solution. At high Péclet numbers, due to increased dispersivity, mass accumulation is possible at the domain edges. Hence, the zero-flux condition that was applied at the domain edges could contribute to an error in the dispersion coefficient calculation. The problem is exacerbated by the x^2 term in Eq. 25 as minor disturbances in concentration at the domain edges contribute greatly to the error. The effect of side walls was examined by Pagistas et al.[43] for Taylor dispersion of a solute accompanying Poiseuille-like laminar flow through a rectangular duct of small aspect ratio. It was shown that in the limit of vanishing aspect ratio, the long-time Taylor dispersivity is nearly eight times larger than that which exists for the comparable 1-D Poiseuille flow between parallel plates in the absence of side walls. This would imply that the effect of the side walls could result in significant overprediction of the dispersivities. The analytical solution is a limiting approximation as well, so the baseline for comparison, which is the analytical solution in this case, is not entirely accurate. Given the above limitations of the test method, even though the errors were high at high $P\acute{e}$, for complex problems such as drug dispersion in the sloshing vitreous, the error was deemed acceptable in exchange for the speedup.

Intravitreal transport

One of the main physiological functions of the vitreous is to act as a barrier for heat and mass transport between the anterior and the posterior eye. With the breakdown of the vitreous from its gel state, the barrier is breached. Hence, vitreous liquefaction could potentially affect intravitreal drug transport heavily.[44,45] The problem becomes doubly important given that a majority of patients with certain posterior-segment diseases, e.g., age-related macular degeneration, have a partially or totally liquefied vitreous because of their age. Many drug delivery systems are based on controlled release mechanisms, intended to deliver the drug over a long period of time.[46] Hence, long-time simulation of drug transport in the vitreous is important to determine drug concentrations at the target tissues. The numerical scheme developed for simulating transport in this article is ideally suited for this problem given the complex geometry of the posterior eye, high Péclet number transport ($\sim 10^6$), time-scale separation between the convective and diffusive component of transport, and the oscillatory nature of flow involved.

Our results suggest that there are significant differences in drug transport between the sloshing and static vitreous.

Increased mixing of the drug resulted in easier access to the clearance routes (retina and hyaloid) resulting in reduced half-lives for the drug in the vitreous. The timescale for transport determines the dosing frequency. For invasive procedures such as intravitreal injections, where patient tolerances are typically low and side-effect risk is considerable, knowing the transport timescale would allow better management of the therapy. The following references highlight the time scale for transport of drugs for different disease states.[47–51] Time scales are also critical factors in the design of controlled release drug sources. From a clinical perspective, increased clearance through the retina and the hyaloid could be significant as well. This would suggest significant drug accumulation in those areas resulting in possible side effects. Also, increased macular concentrations for the sloshing case could cause a supposedly nontoxic dosage of drug to treat macular degeneration to become toxic when the vitreous is liquefied and sloshing.

The results discussed above highlight the importance of the model for a complex problem like drug dispersion in the sloshing vitreous. The method used to develop the model is highly useful for our problem of interest, as it can help understand the balance in transport rates for drug in the sloshing eye. The limitations of the method, that have been highlighted, should be kept in mind while interpreting the results. The model might overpredict diffusion and hence underestimate the time scale for transport. In its current state, the model is more of a guiding tool for design, and is less of a predictive tool. Hence, it should be used purely to gauge trends in drug distribution with the ultimate goal being, to assess efficacy and toxicity for various drug delivery systems for design optimization purposes. The method proposed in this article helps to achieve that goal.

In conclusion, a numerical scheme was developed to simulate dispersion induced by a rapidly oscillating velocity field, in complex geometries, when the convection and diffusion time scales are widely separated. The performance of the method was assessed by comparing numerical results with the analytical solution for a test problem. The implicit telescopic envelope-tracking scheme was found to be effective in bridging the time scales, and the results show that useful speedups ($\sim$100-fold for intravitreal drug transport) can be achieved with minimal compromise on accuracy, once the initial transients stabilize. The method, when used to simulate the test problem, produced overdispersive solutions at high Péclet numbers. However, it should be noted that external factors, other than the method itself, could contribute to the errors observed. The performance of the method was deemed to be satisfactory for our problem of interest. Also, as better methods for high-Pé simulations evolve, they could be combined with the telescopic approach. When extending the method to other problems though, one should be mindful of the limitations of the method, which is best suited for moderate Péclet numbers, rapid oscillations, and large differences in time scale. It is critical to consider how the method would fare when answering specific problem objectives before utilizing it.

Acknowledgments

Literature Cited

1. Taylor G. Dispersion of soluble matter in solvent flowing slowly through a tube. *R Soc Lond Proc Ser A Math Phys Eng Sci*. 1953;219:186–203.
2. Gill W. Analysis of axial dispersion with time variable flow. *Chem Eng Sci*. 1967;22:1013–1017.
3. Harris HG, Goren SL. Axial diffusion in a cylinder with pulsed flow. *Chem Eng Sci*. 1967;22:1571–1576.
4. Horn F, Kipp R. Induced transport in pulsating flow. *AIChE J*. 1971;17:621–626.
5. Knobloch E, Merryfield W. Enhancement of diffusive transport in oscillatory flows. *Astrophys J*. 1992;401:196–205.
6. Tsangaris S. Longitudinal dispersion in a duct with moving walls. *Z Angew Math Phys*. 1986;37:895–909.
7. Watson E. Diffusion in oscillatory pipe flow. *J Fluid Mech*. 1983;133:233–244.
8. Aris R. On the dispersion of a solute in pulsating flow through a tube. *R Soc Lond Proc Ser A Math Phys Eng Sci*. 1960;259:370–376.
9. Horn F, Kipp K Jr. Mass transport under oscillatory fluid flow conditions. *Chem Eng Sci*. 1967;22:1879–1880.
10. Grotberg JB. Respiratory fluid mechanics and transport processes. *Annu Rev Biomed Eng*. 2001;3:421–457.
11. Grotberg J. Pulmonary flow and transport phenomena. *Annu Rev Fluid Mech*. 1994;26:529–571.
12. Jaeger MJ, Kalle P, Kurzweg UH. Separation of gases by enhanced upstream diffusion. *Sep Sci Technol*. 1992;27:691–702.
13. Slutsky A, Drazen F, Ingram R, Kamm R, Shapiro A, Fredberg J, Loring S, Lehr J. Effective pulmonary ventilation with small-volume oscillations at high frequency. *Science*. 1980;209:609–671.
14. Khoo M, Slutsky A, Drazen J, Solway J, Gavriely N, Kamm R. Gas mixing during high-frequency ventilation: an improved model. *J Appl Physiol*. 1984;57:493–506.
15. Nishida M, Inaba Y, Tanishita K. Gas dispersion in a model pulmonary bifurcation during oscillatory flow. *J Biomech Eng*. 1997;119:309–316.
16. Scherer P, Shendalman L, Greene N, Bouhuys A. Measurement of axial diffusivities in a model of the bronchial airways. *J Appl Physiol*. 1975;38:719–723.
17. Jaeger MJ. Diffusion and dispersion in steady counterflow a method for the separation of gases using enhanced mass transport in oscillatory flow. *Chem Eng Sci*. 1998;53:3613–3621.
18. Christie I, Griffiths D, Mitchell A, Zienkiewicz O. Finite element methods for second order differential equations with significant first derivatives. *Int J Numer Methods Eng*. 1976;10:1389–1396.
19. Heinrich J, Huyakorn P, Zienkiewicz O, Mitchell A. An 'upwind' finite element scheme for two-dimensional convective transport equation. *Int J Numer Methods Eng*. 1977;11:131–143.
20. Brooks A, Hughes T. Streamline upwind/Petrov-Galerkin formulations for convection dominated flows with particular emphasis on the incompressible Navier-Stokes equations. *Comput Methods Appl Mech Eng*. 1982;32:199–259.
21. Hughes TJR. Recent progress in the development and understanding of SUPG methods with special reference to the compressible Euler and Navier-Stokes equations. *Int J Numer Methods Fluids*. 1987;7:1261–1275.
22. Petzold LR. An efficient numerical method for highly oscillatory ordinary differential equations. *SIAM J Numer Anal*. 1981;18:455–479.
23. White J, Leeb SB. An envelope-following approach to switching power converter simulation. *IEEE Trans Power Electron*. 1991;6:303–307.
24. Kevrekidis IG, Gear CW, Hummer G. Equation-free: the computer-aided analysis of complex multiscale systems. *AIChE J*. 2004;50:1346–1355.
25. Mei T, Roychowdhury J. An efficient and robust technique for tracking amplitude and frequency envelopes in oscillators. *Proc. IEEE International Conference on Computer-Aided Design*. 2005;599–603.
26. Stay MS, Xu J, Randolph TW, Barocas VH. Computer simulation of convective and diffusive transport of controlled-release drugs in the vitreous humor. *Pharm Res*. 2003;20:96–102.
27. Balachandran RK, Barocas VH. Computer modeling of drug delivery to the posterior eye: effect of active transport and loss to choroidal blood flow. *Pharm Res*. 2008;25:2685–2696.
28. Walton KA, Meyer CH, Harkrider CJ, Cox TA, Toth CA. Age-related changes in vitreous mobility as measured by video B scan ultrasound. *Exp Eye Res*. 2002;74:173–180.
29. Repetto R, Stocchino A, Cafferata C. Experimental investigation of vitreous humour motion within a human eye model. *Phys Med Biol*. 2005;50:4729–4743.
30. Repetto R. An analytical model of the dynamics of the liquefied vitreous induced by saccadic eye movements. *Meccanica*. 2006;41:101–117.
31. Gresho PM, Sani RL. *Incompressible Flow and the Finite Element Method*, vols. 1, 2. New York: Wiley, 2000.
32. Gunzburger MD. *Finite Element Methods for Viscous Incompressible Flows: a Guide to Theory, Practice, and Algorithms*. Boston: Academic Press, 1989.
33. Taylor C, Hood P. A numerical solution of the Navier-Stokes equations using the finite element technique. *Comput Fluids*. 1973;1:73–100.
34. Amestoy PR, Duff IS, L'Excellent JY. MUMPS multifrontal massively parallel solver version 2.0. *J Phys Condens Matter*. 1998;10:7975.
35. Hughes TJR. A simple scheme for developing 'upwind' finite elements. *Int J Numer Methods Eng*. 1978;12:1359–1365.
36. Gear C, Kevrekidis I. Telescopic projective integrators for stiff differential equations. *J Comput Phys*. 2003;187:95–109.
37. Saad Y, Schultz MH. GMRES: a generalized minimal residual algorithm for solving nonsymmetric linear systems. *SIAM J Sci Stat Comput*. 1986;7:856–869.
38. Gear CW, Kevrekidis IG. Projective methods for stiff differential equations: problems with gaps in their eigenvalue spectrum. *SIAM J Sci Comput*. 2003;24:1091–1106.
39. Gear C, Kevrekidis IG. Telescopic projective methods for parabolic differential equations. *J Comput Phys*. 2003;187:95–109.
40. Balachandran RK, Barocas VH. Contribution of saccadic motion to intravitreal drug transport: theoretical analysis. *Pharm Res*. 2011;28:1049–1064.
41. Lee B, Litt M, Buchsbaum G. Rheology of the vitreous body. I: Viscoelasticity of human vitreous. *Biorheology (Oxford)*. 1992;29:521–533.
42. Becker W. The neurobiology of saccadic eye movements. Metrics. *Rev Oculomot Res*. 1989;3:13–67.
43. Pagitsas M, Nadim A, Brenner H. Multiple time scale analysis of macrotransport processes. *Phys A Stat Mech Appl*. 1986;135:533–550.
44. Chin H, Park T, Moon Y, Oh J. Difference in clearance of intravitreal traimcinolone acetonide between vitrectomized and nonvitrectomized eyes. *Retina*. 2005;25:556.
45. Doft BH, Weiskopf J, Nilsson-Ehle I, Wingard LB Jr. Amphotericin clearance in vitrectomized versus nonvitrectomized eyes. *Ophthalmology*. 1985;92:1601–1605.
46. Yasukawa T, Ogura Y, Tabata Y, Kimura H, Wiedemann P, Honda Y. Drug delivery systems for vitreoretinal diseases. *Prog Retin Eye Res*. 2004;23:253–281.
47. Beer PM, Bakri SJ, Singh RJ, Liu W, Peters GB III, Miller M. Intraocular concentration and pharmacokinetics of triamcinolone acetonide after a single intravitreal injection. *Ophthalmology*. 2003;110:681–686.
48. Donati G. Emerging therapies for neovascular age-related macular degeneration: state of the art. *Ophthalmologica*. 2000;221:366–377.
49. Schindler RH, Chandler D, Thresher R, Machemer R. The clearance of intravitreal triamcinolone acetonide. *Am J Ophthalmol*. 1982;93:415–417.
50. Ficker L, Meredith TA, Gardner S, Wilson LA. Cefazolin levels after intravitreal injection. Effects of inflammation and surgery. *Invest Ophthalmol Vis Sci*. 1990;31:502–505.
51. Aguilar HE, Meredith TA, El-Massry A, Shaarawy A, Kincaid M, Dick J, Ritchie DJ, Reichley RM, Neisman MK. Vancomycin levels after intravitreal injection. Effects of inflammation and surgery. *Retina*. 1995;15:428–432.

Appendix A

Cost of calculating A explicitly

Matrix A is derived from Eq. 15 in the text. For the sake of convenience, we rename c_n as y_0 and c_{n+1} as y_m for the derivation (Figure 2).

$$y_m \equiv c_{n+1} \quad \text{and} \quad y_0 \equiv c_n \qquad \text{(A1)}$$

We also define

$$G \equiv \frac{\partial y_m}{\partial y_0} \qquad (A2)$$

and

$$P_i \equiv \frac{\partial y_i}{\partial y_{i-1}} \qquad (A3)$$

Then

$$A = (M+1)I - MG \qquad (A4)$$

G can then be written as a product of P_i's

$$G = \frac{\partial y_m}{\partial y_{m-1}} \frac{\partial y_{m-1}}{\partial y_{m-2}} \cdots \frac{\partial y_2}{\partial y_1} \frac{\partial y_1}{\partial y_0} = P_m P_{m-1} \cdots P_2 P_1 \qquad (A5)$$

GFEM discretization of Eq. 3 yields a system of equations of the form

$$S_i y_i = b + K y_{i-1} \qquad i = 1, 2, \ldots, m \qquad (A6)$$

where S_i's and K are matrices of size $10^5 \times 10^5$ and y_i's and b are vectors of size $10^5 \times 1$.

Differentiating (A5) with respect to y_{i-1}

$$S_i P_i = K \qquad i = 1, 2, \ldots, m \qquad (A7)$$

Evaluating P_i would involve calculating S_i^{-1} and the product of S_i^{-1} and K. Evaluating G from P_i's would involve m-1 matrix-matrix products. Hence, to compute A (Eq. A4), a total of m inverse operations and 2m-1 matrix-matrix products have to be performed.